

Probing a single nuclear spin in a silicon single electron transistor

F. Delgado, R. Aguado, and J. Fernández-Rossier

Citation: *Appl. Phys. Lett.* **101**, 072407 (2012); doi: 10.1063/1.4746260

View online: <http://dx.doi.org/10.1063/1.4746260>

View Table of Contents: <http://apl.aip.org/resource/1/APPLAB/v101/i7>

Published by the [American Institute of Physics](http://www.aip.org).

Related Articles

One electron-based smallest flexible logic cell

Appl. Phys. Lett. **101**, 183101 (2012)

Charge sensing in a Si/SiGe quantum dot with a radio frequency superconducting single-electron transistor

Appl. Phys. Lett. **101**, 142103 (2012)

Spin gating electrical current

Appl. Phys. Lett. **101**, 122411 (2012)

Single charge detection in capacitively coupled integrated single electron transistors based on single-walled carbon nanotubes

Appl. Phys. Lett. **101**, 123506 (2012)

Tunable aluminium-gated single electron transistor on a doped silicon-on-insulator etched nanowire

Appl. Phys. Lett. **101**, 103504 (2012)

Additional information on *Appl. Phys. Lett.*

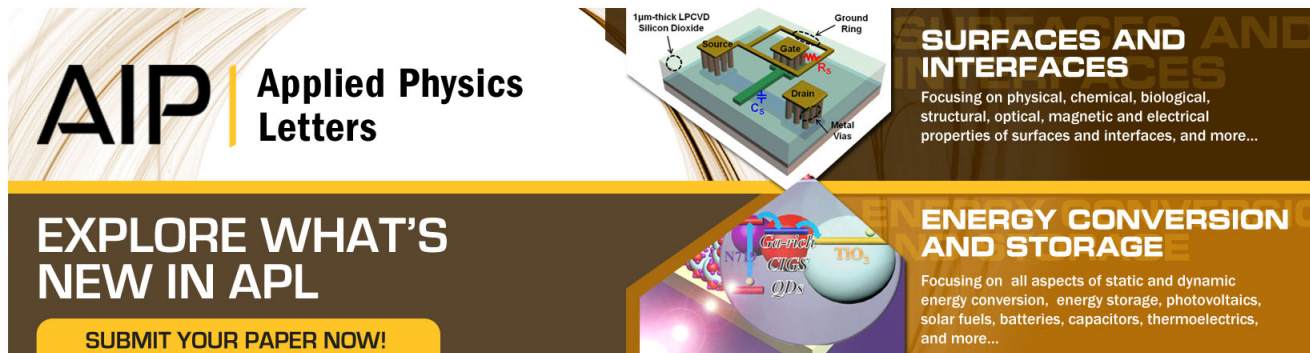
Journal Homepage: <http://apl.aip.org/>

Journal Information: http://apl.aip.org/about/about_the_journal

Top downloads: http://apl.aip.org/features/most_downloaded

Information for Authors: <http://apl.aip.org/authors>

ADVERTISEMENT



AIP | Applied Physics
Letters

EXPLORE WHAT'S NEW IN APL

SUBMIT YOUR PAPER NOW!

SURFACES AND INTERFACES
Focusing on physical, chemical, biological, structural, optical, magnetic and electrical properties of surfaces and interfaces, and more...

ENERGY CONVERSION AND STORAGE
Focusing on all aspects of static and dynamic energy conversion, energy storage, photovoltaics, solar fuels, batteries, capacitors, thermoelectrics, and more...

Labels in diagrams: 1µm-thick LPCVD Silicon Dioxide, Source, Drain, Metal Vias, Ground Ring, QDs, CNTs, CIGS, NO₂.

Probing a single nuclear spin in a silicon single electron transistor

F. Delgado,¹ R. Aguado,² and J. Fernández-Rossier^{1,3}

¹International Iberian Nanotechnology Laboratory (INL), Av. Mestre José Veiga, 4715-330 Braga, Portugal

²Instituto de Ciencia de Materiales de Madrid (ICMM-CSIC), Cantoblanco, 28049 Madrid, Spain

³Departamento de Física Aplicada, Universidad de Alicante, 03690 San Vicente del Raspeig, Spain

(Received 11 July 2012; accepted 2 August 2012; published online 16 August 2012)

We study single electron transport across a single Bi dopant in a silicon nanotransistor to assess how the strong hyperfine coupling with the Bi nuclear spin $I=9/2$ affects the transport characteristics of the device. In the sequential tunneling regime we find that at, temperatures in the range of 100 mK, dI/dV curves reflect the zero field hyperfine splitting as well as its evolution under an applied magnetic field. Our non-equilibrium quantum simulations show that nuclear spins can be partially polarized parallel or antiparallel to the electronic spin just tuning the applied bias.

© 2012 American Institute of Physics. [<http://dx.doi.org/10.1063/1.4746260>]

The amazing progress both in the silicon processing technologies and in the miniaturization of silicon based transistors has reached the point where single-dopant transistors have been demonstrated.^{1–8} Whereas this progress has been fueled by the development of classical computing architectures, it might also be used for donor based quantum computing. In this regard, the electronic and nuclear spins of single donors in silicon are very promising building blocks for quantum computing.^{9–14} Progress along this direction makes it necessary to implement single spin readout schemes both for electronic and nuclear spins. Single electronic spin readout has been demonstrated, both in GaAs quantum dots as well as in P doped silicon nanotransistors.^{15,16}

The readout of the quantum state of a single nuclear spin, much more challenging, has been demonstrated for NV centers in diamond taking advantage of single spin optically detected magnetic resonance afforded by the extraordinary properties of that system.¹⁷ Single nuclear spin readout with either optical¹⁸ or a combined electro-optical techniques¹⁹ has been proposed, but remains to be implemented. Here we explore the electrical readout of a single nuclear spin, more suitable for an indirect band-gap host like Si. A preliminary step is to construct a circuit whose transport is affected by the quantum state of the nuclear spin. There is ample experimental evidence of the mutual influence of many nuclear spins and transport electrons in III-V semiconductor quantum dots in the single electron transport regime.^{20–23} In particular, Kobayashi *et al.* have reported hysteresis in the dI/dV upon application of magnetic fields, reflecting the realization of different ensemble of nuclear states coupled to the electronic spin via hyperfine coupling.²³

Here we propose a device where a single nuclear spin is probed in single electron transport. We model the single electron transport in a silicon nanotransistor such that, in the active region, transport takes place through a single Bi dopant, see Fig. 1. We show that, at sufficiently low temperatures, the dI/dV curves of this device probe the hyperfine structure of the dopant level. In turn, the occupations of the nuclear spin states are affected by the transport electrons. Whereas single dopant transistors have been demonstrated for single P, As and B, in Si,^{4,5,7,16} we choose Bi because it has a much larger hyperfine splitting,^{24–26} due to both a

larger nuclear spin $I=9/2$ and a larger hyperfine coupling constant ($A \approx 6.1 \mu\text{eV}$). The zero-field splitting of the Bi donor level is given by $5A$ and has been observed by electron spin resonance^{24–26} and in photoluminescence experiments with many dopants.²⁷

We consider the sequential transport regime, where the occupation of the donor level fluctuates between $q=0$ and $q=1$. In the $q=0$ state, the nuclear spin interacts only with the external field. In the $q=1$ state, the electron and the nuclear spin are hyperfine coupled. The Hamiltonian that describes both states reads^{24–26,28}

$$\mathcal{H} = q(\epsilon_d + eV_G + A\vec{S} \cdot \vec{I} + \hbar\omega_e S_z) + \hbar\omega_N I_z, \quad (1)$$

where ϵ_d is the donor energy level with respect to the Fermi energy, which we take as $E_F = 0$, and V_G denotes an external gate voltage. We assume that valley degeneracies of the donor level are split-off and neglect the valley degree of freedom. The third term is the hyperfine coupling, and the last two, where $\hbar\omega_e = g_e \mu_B B_z$ and $\hbar\omega_N = g_n \mu_N B_z$, correspond to the electron and nuclear Zeeman terms, with g_e (g_n) the electron (nuclear) g-factors and μ_B (μ_N) the Bohr (nuclear) magneton. In equilibrium, i.e., at zero bias, the occupation of the dopant level depends on the value of the addition energy, which ignoring the Zeeman terms and the tiny correction due to the hyperfine coupling, is given by $\epsilon_0(V_G) \equiv \epsilon_d + eV_G$.

We denote the $q=0$ eigenstates as $|m\rangle$. Their energies read as $\epsilon_m \equiv \hbar\omega_N I_z$. The eigenenergies and eigenvectors of $q=1$ are denoted by ϵ_M and $|M\rangle$. The $q=1$ zero-field Hamiltonian $A\vec{I} \cdot \vec{S}$ can be diagonalized in terms of the total angular operator F , resulting in two multiplets ($F=4$, $F=5$) with energies $E_{F=4} = -11A/4$ and $E_{F=5} = 9A/4$, and a zero-field splitting $\Delta_0 = 5A \approx 30 \mu\text{eV}$. At finite magnetic field, the exact eigenvalues of \mathcal{H} can also be calculated analytically.²⁶ The corresponding energy levels are shown in Fig. 2.

The tunneling Hamiltonian between the single Bi dopant level and the source and drain electrodes reads as

$$\mathcal{H}_{\text{tun}} = \sum_{\lambda\sigma} V_{\lambda} (d_{\sigma}^{\dagger} c_{\lambda\sigma} + h.c.), \quad (2)$$

where operator $c_{\lambda,\sigma}$ annihilates an electron with spin σ and orbital quantum number $\lambda \equiv \eta, \vec{k}$, with wave vector \vec{k} and

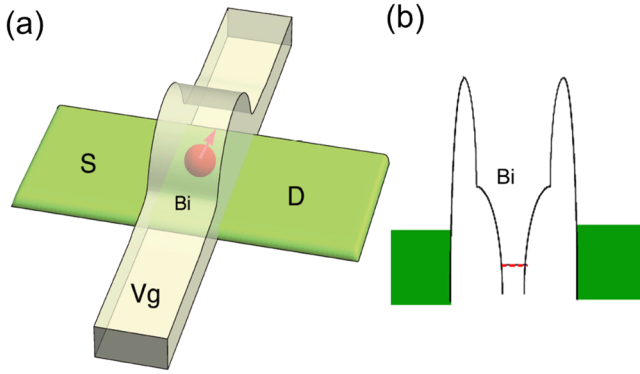


FIG. 1. (a) Scheme of the Si:Bi FinFET nanotransistor. (b) Trapping Coulomb potential of the Bi dopant a single energy level participating in the transport.

electrode index $\eta = S, D$, while operator d_σ annihilates a spin σ electron in the dopant level. The scattering rate for the tunneling process, ignoring the hyperfine coupling, is given by $\Gamma_0^\eta = \frac{2\pi}{\hbar} |V_\eta|^2 \rho_\eta$, where ρ_η is the density of states of the electrode. Our model is very similar to the one used to describe single electron transport through a quantum dot exchanged coupled to a single Mn atom.^{29,30}

The dissipative dynamics of the electro-nuclear spin system under the influence of the coupling to the electrodes is described by a Bloch-Redfield (BR) master equation.^{30,31} The coupling to the reservoir, given by the tunneling Hamiltonian, involves transitions between the $q=0$ and $q=1$ manifolds. The corresponding transition rates are calculated using the Fermi golden rule with \mathcal{H}_{tun} as the perturbation,³⁰

$$\Gamma_{m,M}^\eta = \Gamma_0^\eta \sum_\sigma |\langle M | I_z(m), \sigma \rangle|^2, \quad (3)$$

where $|I_z, \sigma\rangle \equiv |I_z\rangle \otimes |\sigma\rangle$. In the following we take the applied bias convention $\mu_S - \mu_D = eV$, with $\mu_S = eV/2$ and $\mu_D = -eV/2$. For a given temperature, bias and gate voltages and Hamiltonian parameters, we obtain the steady state solution of the master equation, ignoring the effect of the fast-decaying coherences. This yields the steady state occupations $P_m(V)$ and $P_M(V)$.

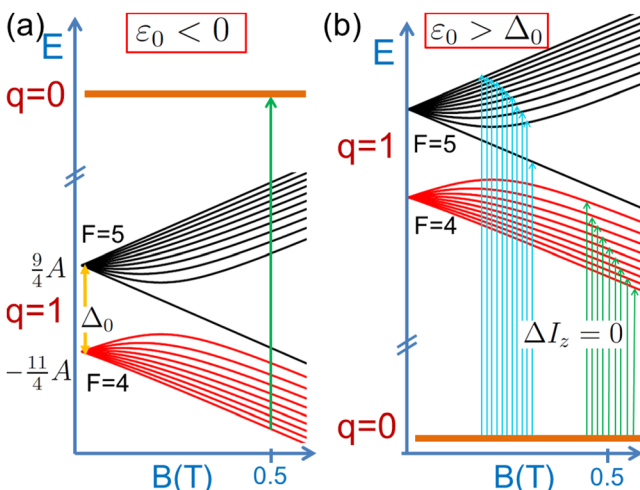


FIG. 2. Scheme of the current-induced allowed transition for the (a) $q=1$ charged system and (b) $q=0$ uncharged system. It has been assumed that $\hbar\omega_N \ll k_B T \ll \hbar\omega_e \leq \Delta_0$.

We consider the sequential tunneling regime, in which the energy level broadening induced by coupling to the electrodes Γ_0 is small, $\hbar\Gamma_0 \ll k_B T$. This also justifies the Markovian approximation implicit in the Bloch-Redfield master equation. In this regime, current flows when the bias enables charge fluctuations of the dopant level. The steady state current corresponding to electrons flowing from the source electrode to the dopant level is given by

$$I = e \sum_{m,M} \{ P_m(V) f_S(\Delta_{M,m}) \Gamma_{m,M}^S - P_M(V) [1 - f_S(\Delta_{M,m})] \Gamma_{m,M}^S \}, \quad (4)$$

where $\Delta_{M,m} = \epsilon_M - \epsilon_m$ and $f_S(\epsilon) = f(\epsilon - \mu_S)$ is the Fermi function relative to the chemical potential of the S electrode. The first term in the right hand-side of Eq. (4) represents the electrons flowing from the S electrode to the empty Bi, while the second one corresponds to electrons flowing from the $q=1$ Bi to the S electrode. In steady state, the continuity equation ensures that current between the dopant and the drain is the same than the source-dopant current.

Figure 3(a) shows the differential conductance dI/dV map for zero-applied magnetic field, with $I = I/(e\Gamma_0)$ and $\Gamma_0^\eta = \Gamma_0/2$. At zero bias, the conductance is zero except at the special value of V_G for which the addition energy vanishes. Far from this point, the zero-bias charge of the dopant state, hereafter denoted with q_0 , is either $q_0 = 0$ or $q_0 = 1$. The finite bias conductance has a peak whenever the bias energy, $eV/2$, matches the energy difference between two states with different charge, m for $q=0$ and M for $q=1$, that are permitted by the spin selection rule implicit in Eq. (3). The height of the peak is proportional to both the non-equilibrium occupations P_m and P_M and to the quantum mechanical matrix element $\Gamma_{m,M}^\eta$. This determines the very different spectra when the zero bias charge in the dopant is $q=0$ or $q=1$. The width of the dI/dV peaks is proportional to $k_B T$, so that the dI/dV spectra can resolve the hyperfine structure provided that $k_B T$ is smaller than the splitting of the levels. The energy differences inside the $F=4$ and $F=5$ manifolds, see Fig. 2, are roughly proportional to A . Thus, while the zero-field splitting can be resolved at $T=0.3$ K, temperature must be significantly below 50 mK to resolve the finite field structure, see Fig. 3(c).

Let us consider first the $q_0 = 1$ case (left panel in Fig. 3). At 10 mK, only the ground state(s) is (are) occupied. Thus, a single transition is seen, from the $q=1$ to the $q=0$ states. As the magnetic field is ramped, the energy of the transition increases, reflecting the electronic Zeeman shift. In contrast, in the $q_0 = 0$ case (right panel in Fig. 3), all the Zeeman split nuclear levels are equally populated, even down to mK temperatures. Spin conservation selection rule implicit in Eq. (2) connects these 10 quasi-degenerate states of the $q=0$ manifold to the hyperfine spin-split levels of the $q=1$ manifold with different energies. As a result, the dI/dV curve reveals 2 peaks at zero field, reflecting the splitting between the $F=4$ and $F=5$ states. At higher fields, the two zero-field peaks split in up to 10 peaks that can be resolved at low enough temperature [see Figs. 3(c) and 4(b)].

Interestingly, the application of a bias to the $q_0 = 0$ state, for which the nuclear spin states are randomized, can result in

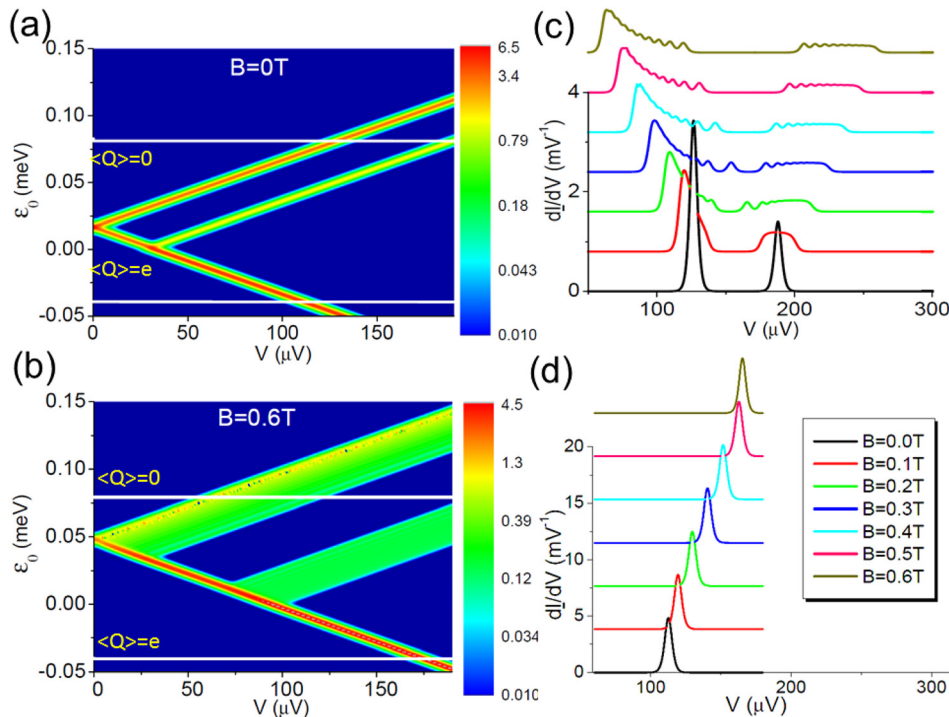


FIG. 3. (a) and (b) Contour plot of the dI/dV vs. applied bias V and on-site energy ϵ_0 at zero magnetic field and $B=0.6$ T, respectively. (c) and (d) Conduction spectrum dI/dV as a function of applied bias for different magnetic fields at $\epsilon_0 = -0.4$ meV and $\epsilon_0 = 0.8$ meV respectively. White horizontal lines in panel (a) and (b) marks the values of ϵ_0 in the 2D plots (c) and (d). In all cases, $T = 10$ mK and $\hbar\Gamma_0 = 0.1 \mu\text{eV}$.

a finite average nuclear magnetic moment. We show this in Fig. 4(a) for finite B . At zero bias, the charge of the dopant level is $q_0 = 0$, and the nuclear spins are randomized. When the bias hits the addition energy a selective depopulation of a given I_z level of the $q=0$ manifold starts, in favor of a $q=1$ state that mixes the I_z and $I_z \pm 1$ components, resulting in a net accumulation of nuclear spin. When all the transitions to the $F=4$ manifold are allowed, the nuclear spin vanishes again. Then, when the bias permits the transitions to the $F=5$ manifold, the nuclear spin accumulation starts in the opposite direction. Thus, when $|eV/2|$ matches the center of the $F=4$ multiplet, see Fig. 4(a), the nuclear spins tend to align antiparallel to the electronic spin. Then, when $|eV/2|$ reaches the center of the $F=5$ multiplet, the nuclear spins prefer aligning parallel to the electronic spin.

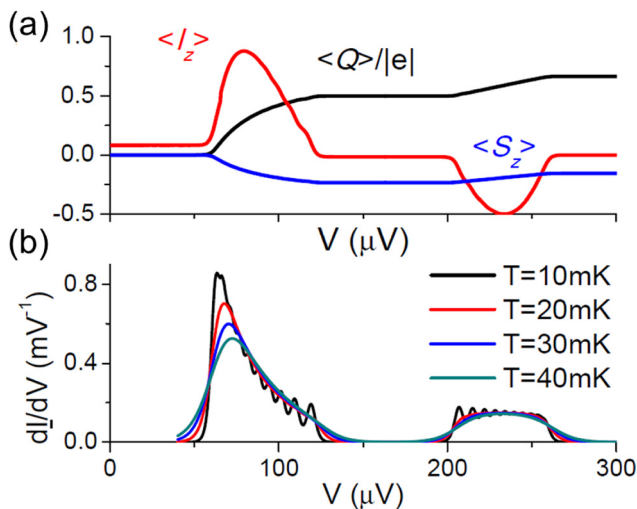


FIG. 4. (a) Average electronic occupation of the Bi, $\langle Q \rangle / |e|$ (black line) and nuclear and electronic spins, $\langle I_z \rangle$ (red line) and $\langle S_z \rangle$ (blue line), respectively. (b) dI/dV vs. bias for different temperatures. Same parameters as Fig. 3(c) with $B = 0.6$ T.

Whereas all our results discussed so far refer to steady state conditions, it is worth pointing out that there are two very different time scales in the dynamics of the system. Whereas the charge equilibrates in the dopant level in a time scale set by $1/\Gamma_0$, the nuclear spin relaxation, dominated by many events of hyperfine exchange with the electronic spin and subsequent recharging of the Bi,³² takes place at a much longer time scale, hundreds of times larger than $1/\Gamma_0$, but still much shorter than the intrinsic T_1 time of the nuclear spin. Thus, charge fluctuations in the Bi induce nuclear spin relaxation.³²

We finally discuss the experimental feasibility of our proposal with state of the art techniques. First, according to our simulations, see Fig. 4(b), the finite field hyperfine splitting is resolved at 10 mK but not a 20 mK. At 40 mK the 2 humps associated to the $F=4$ and $F=5$ manifolds are clearly resolved. Keeping the transport in the sequential tunneling regime requires that $\hbar\Gamma_0 \ll k_B T$, which at 10 mK, translates into $I \ll 200$ pA. This is within reach of experimental setups.^{16,20,23,33,34}

In conclusion, we have studied the single electron transport spectroscopy of the hyperfine structure of a Bi dopant in a silicon nanotransistor. We have shown that, at sufficiently low temperatures, and when the dopant is ionized with a gate, the dI/dV corresponding to sequential transport can resolve the hyperfine spectrum of the electron in the donor level. In addition, the non-equilibrium transport at finite field results in a hyper polarization of the nuclear spin state, or nuclear spin accumulation. These results are different from our previous work, where we considered the same system in a different transport regime, cotunneling, and we showed that inelastic cotunneling of the dopant in the $q=1$ state could also resolve the hyperfine spectrum and drive the nuclear spin states out of equilibrium.²⁸ Future work should determine how, in the cotunneling regime, the appearance of the Kondo effect⁸ competes with the reported effect.

This work has been financially supported by MEC-Spain (Grant Nos. FIS2010-21883-C02-01, FIS2009-08744, and CONSOLIDER CSD2007-0010) as well as Generalitat Valenciana, Grant Prometeo 2012-11.

- ¹H. Sellier, G. P. Lansbergen, J. Caro, S. Rogge, N. Collaert, I. Ferain, M. Jurczak, and S. Biesemans, *Phys. Rev. Lett.* **97**, 206805 (2006).
- ²G. Lansbergen, R. Rahman, C. Wellard, I. Woo, J. Caro, N. Collaert, S. Biesemans, G. Klimeck, L. Hollenberg, and S. Rogge, *Nature Physics* **4**, 656 (2008).
- ³M. Pierre, R. Wacquez, X. Jehl, M. Sanquer, M. Vinet, and O. Cueto, *Nature Nanotechnol.* **5**, 133 (2009).
- ⁴G. P. Lansbergen, G. C. Tettamanzi, J. Verduijn, N. Collaert, S. Biesemans, M. Blaauboer, and S. Rogge, *Nano Lett.* **10**, 455 (2010).
- ⁵K. Y. Tan, K. W. Chan, M. Mottonen, A. Morello, C. Yang, J. van Donkelaar, A. Alves, J.-M. Pirkkalainen, D. N. Jamieson, R. G. Clark *et al.*, *Nano Lett.* **10**, 11 (2010).
- ⁶V. N. Golovach, X. Jehl, M. Houzet, M. Pierre, B. Roche, M. Sanquer, and L. I. Glazman, *Phys. Rev. B* **83**, 075401 (2011).
- ⁷M. Fuechle, J. A. Miwa, S. Mahapatra, H. Ryu, S. Lee, O. Warschkow, L. C. L. Hollenberg, G. Klimeck, and M. Y. Simmons, *Nature Nanotechnol.* **7**, 242 (2012).
- ⁸G. C. Tettamanzi, J. Verduijn, G. P. Lansbergen, M. Blaauboer, M. J. Calderón, R. Aguado, and S. Rogge, *Phys. Rev. Lett.* **108**, 046803 (2012).
- ⁹B. Kane, *Nature* **393**, 133 (1998).
- ¹⁰D. P. DiVincenzo, D. Bacon, J. Kempe, G. Burkard, and K. B. Whaley, *Nature* **408**, 339 (2000).
- ¹¹R. Vrijen, E. Yablonovitch, K. Wang, H. W. Jiang, A. Balandin, V. Roychowdhury, T. Mor, and D. DiVincenzo, *Phys. Rev. A* **62**, 012306 (2000).
- ¹²R. de Sousa, J. D. Delgado, and S. Das Sarma, *Phys. Rev. A* **70**, 052304 (2004).
- ¹³L. C. L. Hollenberg, A. D. Greentree, A. G. Fowler, and C. J. Wellard, *Phys. Rev. B* **74**, 045311 (2006).
- ¹⁴T. D. Ladd, F. Jelezko, R. Laflamme, Y. N. Y. C. Monroe, and J. L. O'Brien, *Nature* **464**, 45 (2010).
- ¹⁵J. M. Elzerman, R. Hanson, L. H. W. van Beveren, B. Witkamp, L. M. K. Vandersypen, and L. P. Kouwenhoven, *Nature* **430**, 431 (2004).
- ¹⁶A. Morello, J. J. Pla, F. A. Zwanenburg, K. W. Chan, K. Y. Tan, H. Huebl, M. Möttönen, C. D. Nugroho, C. Yang, J. A. van Donkelaar *et al.*, *Nature* **467**, 687 (2010).
- ¹⁷P. Neumann, J. Beck, M. Steiner, F. Rempp, H. Fedder, P. R. Hemmer, J. Wrachtrup, and F. Jelezko, *Science* **329**, 542 (2010).
- ¹⁸K.-M. C. Fu, T. D. Ladd, C. Santori, and Y. Yamamoto, *Phys. Rev. B* **69**, 125306 (2004).
- ¹⁹D. Sleiter, N. Y. Kim, K. Nozawa, T. D. Ladd, M. L. W. Thewalt, and Y. Yamamoto, *New J. Phys.* **12**, 093028 (2010).
- ²⁰J. R. Petta, J. M. Taylor, A. C. Johnson, A. Yacoby, M. D. Lukin, C. M. Marcus, M. P. Hanson, and A. C. Gossard, *Phys. Rev. Lett.* **100**, 067601 (2008).
- ²¹D. J. Reilly, J. M. Taylor, J. R. Petta, C. M. Marcus, M. P. Hanson, and A. C. Gossard, *Science* **321**, 817 (2008).
- ²²S. Foletti, H. Bluhm, D. Mahalu, V. Umansky, and A. Yacoby, *Nature Phys.* **5**, 903 (2009).
- ²³T. Kobayashi, K. Hitachi, S. Sasaki, and K. Muraki, *Phys. Rev. Lett.* **107**, 216802 (2011).
- ²⁴R. E. George, W. Witzel, H. Riemann, N. V. Abrosimov, N. Nötzel, M. L. W. Thewalt, and J. J. L. Morton, *Phys. Rev. Lett.* **105**, 067601 (2010).
- ²⁵G. W. Morley, M. Warner, A. M. Stoneham, P. T. Greenland, J. van Tol, C. W. M. Kay, and G. Aeppli, *Nature Mater.* **9**, 725 (2010).
- ²⁶M. H. Mohammady, G. W. Morley, and T. S. Monteiro, *Phys. Rev. Lett.* **105**, 067602 (2010).
- ²⁷T. Sekiguchi, M. Steger, K. Saeedi, M. L. W. Thewalt, H. Riemann, N. V. Abrosimov, and N. Nötzel, *Phys. Rev. Lett.* **104**, 137402 (2010).
- ²⁸F. Delgado and J. Fernández-Rossier, *Phys. Rev. Lett.* **107**, 076804 (2011).
- ²⁹A. L. Efros, E. I. Rashba, and M. Rosen, *Phys. Rev. Lett.* **87**, 206601 (2001).
- ³⁰J. Fernández-Rossier and R. Aguado, *Phys. Rev. Lett.* **98**, 106805 (2007).
- ³¹C. Cohen-Tannoudji, G. Grynberg, and J. Dupont-Roc, *Atom-Photon Interactions* (Wiley, New York, 1998).
- ³²L. Besombes, Y. Leger, J. Bernos, H. Boukari, H. Mariette, J. P. Poizat, T. Clement, J. Fernández-Rossier, and R. Aguado, *Phys. Rev. B* **78**, 125324 (2008).
- ³³J. Baugh, Y. Kitamura, K. Ono, and S. Tarucha, *Phys. Rev. Lett.* **99**, 096804 (2007).
- ³⁴T. S. Jespersen, K. Grove-Rasmussen, J. Paaske, K. Muraki, T. Fujisawa, J. Nygård, and K. Flensberg, *Nature Phys.* **7**, 348 (2011).